

Cite this: *Soft Matter*, 2012, **8**, 5687

www.rsc.org/softmatter

PAPER

Mechanisms of multi-shape memory effects and associated energy release in shape memory polymers

Kai Yu,^a Tao Xie,^b Jinsong Leng,^c Yifu Ding^a and H. Jerry Qi^{*,a}

Received 9th February 2012, Accepted 19th March 2012

DOI: 10.1039/c2sm25292a

Shape memory polymers have attracted increasing research interest due to their capability of fixing a temporary shape and associated deformation energy then releasing them later on demand. Recently, it has been reported that polymers with a broad thermomechanical transition temperature range can demonstrate a multi-shape memory effect (m-SME), where shape recovery and energy release occur in a stepped manner during free recovery. This paper investigated the underlying physical mechanisms for these observed shape memory behaviors and the associated energy storage and release by using a theoretical modeling approach. A multibranch model, which is similar to the generalized standard linear solid model of viscoelasticity, was used for a quantitative analysis. In this model, individual nonequilibrium branches represent different relaxation modes of polymer chains with different relaxation times. As the temperature was increased in a staged manner, for a given temperature, different numbers of branches (or relaxation modes) became shape memory active or inactive, leading to the observed m-SME. For energy release during free recovery, under a tensile deformation of the SMP, stored energy in individual nonequilibrium branches was first transferred into a compressive deformation energy, then gradually declined to zero. Energy release during recovery was a complicated process due to the involvement of multiple relaxation modes.

1. Introduction

Among shape memory materials, shape memory polymers (SMPs) have gained extensive research interest recently due to their excellent properties, such as high strain recovery (up to 400%),¹ low density, low cost, easy shape programming procedure and easy control of recovery temperature. Besides, they are also chemically tunable to achieve biocompatibility and biodegradability. These advantages allow SMPs to stand out in many applications such as microsystem actuation components, biomedical devices, aerospace deployable structures and morphing structures.^{2–6} Previous investigations on SMPs mainly focused on shape fixation, shape recovery, and external stimuli, such as heat,^{7–11} light,^{12–17} magnetic fields,^{18–22} moisture,^{23,24} *etc.*

To expand the application potential of SMPs, recent research efforts have attempted to increase the number of temporary shapes a SMP can memorize in a shape memory cycle. Triple-shape SMPs were successfully achieved by introducing additional

reversible phase transitions.^{25–29} By changing the glass transition of SMPs or adjusting the ratio between the two transition phases, the triple-shape memory effect can also be tunable. Recently, Xie and co-workers showed that upon heating, a perfluorosulfonic acid (PFSA) ionomer, a thermo-plastic SMP with a broad thermal transition temperature range from 55 °C to 130 °C, can demonstrate a multi-shape memory effect (m-SME) in the free recovery process.^{30,31} In addition, it exhibits a temperature memory effect (TME), referring to the phenomenon that the temperature corresponding to the maximum recovery stress in constrained recovery or maximum strain recovery rate roughly equals the deformation temperature during the programming stage.^{33–35} A qualitative analysis was conducted by Huang and Sun³² to reveal the underlying mechanism of m-SME and TME in SMPs. In their discussions, both effects were attributed to the step by step release of the elastic energy in the elastic part of their dual-part unit model. The elastic energy was step by step stored or frozen during cooling.

In general, various thermo-mechanical transitions such as glass transition or melting transition can be utilized for shape memory. For ease of discussion, however, we hereafter refer only to glass transition. For polymers using glass transition to achieve shape memory, the underlying physical mechanism of shape memory effects is the dramatic chain mobility (or relaxation times) change as the temperature traverses the glass transition temperature (T_g). Whilst a variety of constitutive models^{36–40} were developed for SMPs in the past, this mechanism can be

^aDepartment of Mechanical Engineering, University of Colorado, UCB 427, Boulder, CO 80309, USA. E-mail: qih@colorado.edu

^bChemical Sciences and Materials Systems Laboratory, General Motors Research and Development Center, Mail Code: 480-106-224, 30500 Mound Road, Warren, Michigan 48090-9055, USA

^cCentre for Composite Materials, Science Park of Harbin Institute of Technology (HIT), P.O. Box 3011, No. 2 YiKuang Street, Harbin, P.R. China

illustrated by a simple 1D standard linear solid (SLS) model (Fig. 1) of viscoelasticity in an *ad hoc* manner.⁴¹ In Fig. 1, an elastic spring (or an equilibrium branch) is arranged in parallel with a Maxwell element (also called the non-equilibrium branch), which consists of a spring and a dashpot arranged in series. The mechanical properties of the dashpot are characterized by its viscosity or relaxation time, which strongly depends on the temperature and represents the temperature dependent chain mobility. For example, as the temperature crosses the glass transition temperature, the viscosity or relaxation time can change by tens of orders of magnitude. During a shape memory cycle, the first step is to deform the polymer at a temperature higher than its T_g where the viscosity in the dashpot is very low. Therefore, the dashpot does not present much resistance to the deformation and thus develops a viscous strain close to the overall deformation of the material. As a result, the spring attached to the dashpot is in an almost undeformed state and the energy is stored mainly in the equilibrium branch. In the second step, the temperature is lowered to below T_g while the deformation of the SMP is held constant. Decreasing the temperature below T_g leads to a dramatic increase of viscosity in the dashpot. In the third step, the external load is removed at the low temperature. Because the viscosity is extremely high, the Maxwell element behaves like an elastic solid. Unloading will lead to new deformations in both springs in the equilibrium and non-equilibrium branches due to the requirement of force balance. But since the modulus of the spring in the Maxwell element is generally much higher than the spring in the equilibrium branch, the new deformation in the nonequilibrium branch is very small and much of the deformation introduced at the high temperature is fixed. Nonetheless, this causes an energy redistribution among the two springs. It is also noted that in Fig. 1, the deformation in the nonequilibrium is compressive whilst the overall deformation of the material is tensile. In the recovery step (the fourth step), the temperature is raised above T_g . As a result, the viscosity in the dashpot is dramatically decreased, the force in the spring attached to the dashpot drives the viscous strain back to zero, and the shape is recovered. Note that in this illustration, two features in the dashpot play an important role. First, it is the viscous strain that is frozen or memorized. Therefore, allowing the development of viscous strain during the programming step is critical for the subsequent shape recovery behavior.⁴² Second, the dramatic change in viscosity is essential for the shape memory effect. When the viscosity is low, deforming the material allows the development of a large viscous strain; in the subsequent cooling step, viscosity becomes extremely high and thus the viscous strain developed at the high temperature is locked. During recovery, increasing the temperature reduces the viscosity and thus unlocks the viscous strain and recovers the material.

Although the above description assisted by the SLS model of viscoelasticity illustrates the underlying physics of the SM effect well, it is highly simplified. For a real polymer, multiple relaxation processes of the polymer chains undergo a dramatic change as the temperature crosses T_g . In this regard, multibranch models† (resembling the 1D generalized viscoelastic model or

† Here, it should be noted that a limitation of multibranch models is that a connection between the individual branches and the structure of the polymer could be very difficult.

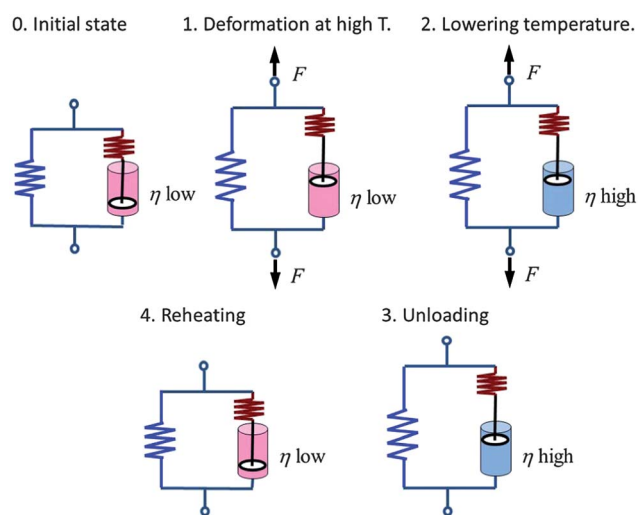


Fig. 1 1D standard linear solid model is used to illustrate the mechanism of shape memory effects in SMP. η represents viscosity.

Prony series) are generally applied. Each branch is taken to represent a relaxation mode, which thus enables the model to capture the overall relaxation in polymers.^{43–46} For example, we have recently demonstrated⁴⁵ that using a KWW stretched exponential function for the relaxation process, one could capture the free and constrained recovery behaviors of an acrylate-based SMP, which has a relatively narrow glass transition temperature (roughly 30 °C to 50 °C). Since the KWW stretched exponential function is equivalent to a generalized viscoelastic model, we recently developed a nonlinear finite deformation thermoviscoelastic model to capture the comprehensive thermomechanical behaviors of the acrylate-based SMPs, including free recovery behaviors at different temperatures.⁴⁶ Compared to the acrylate-based SMPs, the SMP studied by Xie^{30,31} has a much wider thermomechanical transition region, which makes it possible to observe a clear m-SME behavior.

In the study of SMPs, another major concern is the energy storage and release mechanism. It is generally believed that the elastic energy due to deformation above T_g is stored in the polymer as the temperature is lowered to below T_g . During recovery, the stored energy is released and the shape of the material is recovered. Recently, Huang and Sun³² carried out

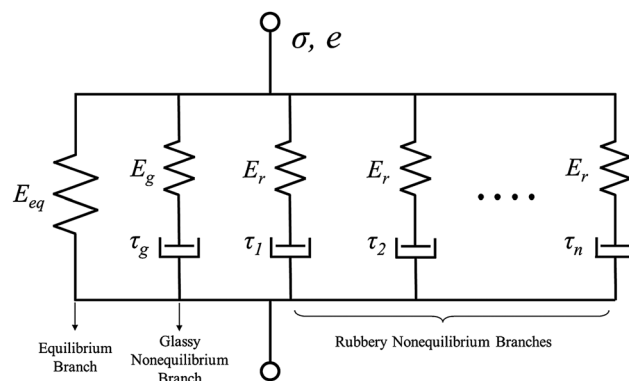


Fig. 2 1D rheological representation of the developed model.

a qualitative analysis to discuss the energy storage and release process. However, as illustrated by the simple 1D SLS model, energy storage is assisted by the evolution of viscous strain in the dashpot and is complicated by the stress relaxation (due to the presence of the dashpot) and by the rebalance of the force during unloading. Therefore, a quantitative analysis supported by material models is necessary.

In this paper, a 1D linear model simplified from our previous 3D nonlinear model is utilized to provide a quantitative understanding of the mechanisms for m-SME. The 1D model was used to fit the experimental results from Xie.^{30,31} The evolution of viscous strain and elastic energy in individual branches was monitored during the shape memory cycles. The underlying energy storage and release mechanisms were then discussed.

2. Constitutive model

A 1D rheological representation of the multibranch model is shown in Fig. 2. The mechanical elements consist of an equilibrium branch and several nonequilibrium branches placed in parallel. The equilibrium branch is a linear spring with a Young's modulus of E_{eq} to represent the equilibrium behavior, and the nonequilibrium branches are Maxwell elements where an elastic spring and a dashpot are placed in series to represent the viscoelastic response. These nonequilibrium branches represent different relaxation processes (or modes) in the polymer system.

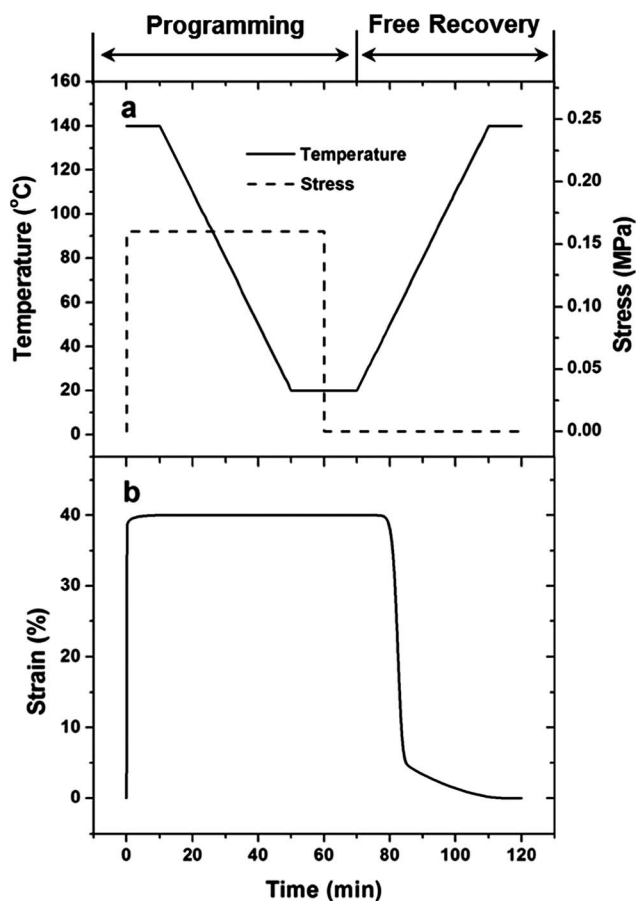


Fig. 3 A simple dual-SM cycle. (a) Temperature and stress history. (b) Simulated strain evolution by using the constructed multibranch model.

In particular, we are interested in the relaxation processes that contribute to the SM effect in the temperature range for a SM cycle. Therefore, among the nonequilibrium branches, one represents the relaxation behavior of the glassy mode. E_g denotes the Young's modulus of the spring and τ_g represents the relaxation time of the dashpot in the glassy branch. The rest of the nonequilibrium branches are used to represent the relaxation modes (for example, Rouse modes) in the rubbery state. In the i -th (i varies from 1 to n) rubbery nonequilibrium branch, the Young's modulus of the spring is always E_r , and the corresponding stress relaxation time of the dashpot is denoted as τ_i , which can be chosen to cover a wide time range with each of them separated by a decade.

In the following, the model is developed under uniaxial small deformation conditions. For the finite deformation model, readers are referred to Westbrook *et al.*⁴⁶ Applying Boltzmann's superposition principle, the total stress is given by

$$\sigma(t) = E_{eq}e(t) + \sum_{i=0}^n E_i \int_0^t \frac{de(s)}{ds} \exp\left(-\frac{t-s}{\tau_i(T)}\right) ds, \quad (1)$$

when $i = 0$, $\tau_i = \tau_g$, and $E_0 = E_g$. In eqn (1), the relaxation times in individual branches vary as the temperature changes. Here, it is assumed that the time-temperature shift for each branch follows the same rule. According to the well-established "thermorheological simplicity" principle,⁴⁷

$$\tau_i(T) = \tau_0^i \alpha_T(T), \quad (2a)$$

$$\tau_g(T) = \tau_0^g \alpha_T(T), \quad (2b)$$

where $\alpha_T(T)$ is the time-temperature superposition shift factor, and τ_0^i and τ_0^g are the reference relaxation times at the temperature when $\alpha_T(T) = 1$.

Following O'Connell and McKenna,⁴⁸ the method for calculating the temperature influence on the viscoelastic behavior depends on whether the material temperature is above or below a temperature T_s . At temperatures above T_s , the Williams-Landel-Ferry (WLF) equation⁴⁹ is used:

$$\log \alpha_T(T) = -\frac{C_1(T - T_M)}{C_2 + (T - T_M)}, \quad (3a)$$

where \log is the base 10 logarithm, C_1 and C_2 are material constants and T_M is the WLF reference temperature. For temperatures below T_s , $\alpha_T(T)$ follows the Arrhenius-type behavior:⁵⁰

$$\ln \alpha_T(T) = -\frac{AF_c}{k_B} \left(\frac{1}{T} - \frac{1}{T_g} \right), \quad (3b)$$

where A and F_c are material constants, and k_B is Boltzmann's constant. T_s is the crossing point of two curves representing eqn (3a) and (3b) on a α_T vs. T plot.

Eqn (1) was solved under the imposed mechanical conditions in a shape memory cycle. In the shape memory cycles studied in this paper, the programming steps were achieved by prescribing the applied stress. Eqn (1) was then solved for $e(t)$ under the condition of $\sigma(t)$ being given. During the free recovery, since there was no force applied to the sample, the total stress was zero. Eqn (1) was solved for $e(t)$ with the left-hand side of the equation being zero. In all these cases, elastic strain e_e^i and viscous strain e_v^i

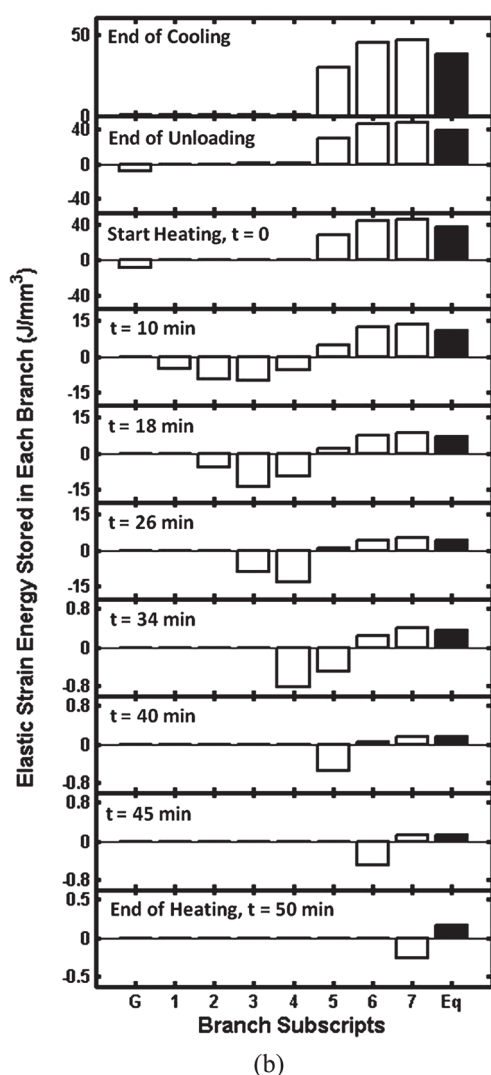
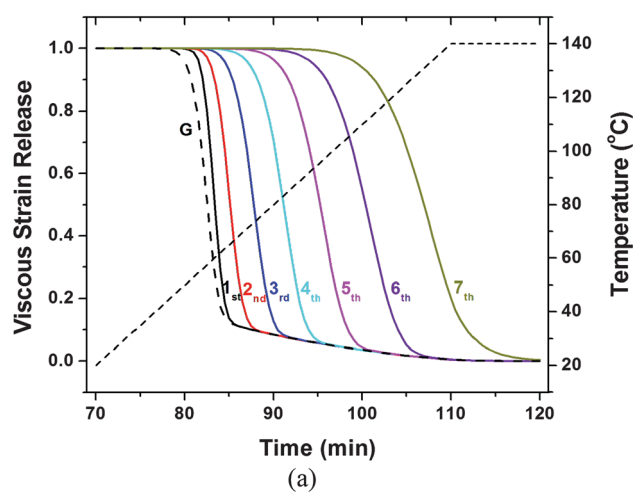


Fig. 4 (a) Strain evolution of dashpots in each rubbery nonequilibrium branch during the free recovery process. Key: solid line, normalized strain release; dotted line, temperature. (b) Elastic strain energy stored in each branch during the free recovery process of SMP. Notes: 1. Subscript “G” denotes the glassy nonequilibrium branch and subscript “Eq” denotes the

(the strain in the dashpot) in individual nonequilibrium branches were given as

$$e_i^e = \int_0^t \frac{de(s)}{dt} \exp\left(-\frac{t-s}{\tau_i(T)}\right) ds, \quad e_i^v = e - e_i^e. \quad (4a)$$

The elastic energy stored in individual branches was calculated as

$$U_i = \frac{1}{2} E_i (e_i^e)^2. \quad (4b)$$

3. Results

The multibranch model was implemented into a MATLAB code. In order to better illustrate the physics revealed by our model, we first present a quantitative analysis for a simple dual-SM cycle, then apply the model to the investigation of triple SME and m-SME which involves much more sophisticated thermo-mechanical loading processes.^{30,31}

3.1 Shape memory effect in a simple SM cycle

For the simple dual-SM cycle, the temperature range was the same as that in Xie’s experiments (20 °C to 140 °C). Fig. 3a shows the thermomechanical loading conditions for this simple SM cycle. In the programming step, the SMP is stretched by a target stress of 0.16 MPa at a temperature of 140 °C. The sample is then cooled to 20 °C with a cooling rate of 3 °C min⁻¹ while the stress is maintained. Ten minutes after the temperature reaches 20 °C, the imposed stress is removed. Ten minutes after the removal of the external load, the SMP is heated to 140 °C with a heating rate of 3 °C min⁻¹ under a stress-free condition. In this simple example, seven rubbery branches were used with the relaxation times evenly distributed within a range of 10⁸ s to 10¹⁴ s, or 1.67 × 10⁶ min to 1.67 × 10¹² min. For simplicity, the relaxation times are reported in minutes in the rest of the paper. The reason for using seven rubbery branches is because, as will be shown later in the paper, a model with seven rubbery branches is identified to be able to capture the m-SME exhibited by the material used in Xie’s experiments. The relaxation time in the glassy branch is 1.67 × 10² min. Fig. 3b shows the variation of strain as a function of temperature. Clearly, at 20 °C, after the removal of the stress, the strain stays constant (or fixed). During free recovery, when the temperature is ramped to 140 °C, the strain gradually decreases to zero, indicating the recovery of the original shape.

Fig. 4a shows the release of viscous strains in nonequilibrium branches during the recovery process. In Fig. 4a, the viscous strain release is defined as the real-time viscous strains normalized by the initial viscous strains at the beginning of the heating process, which are $e_0^{vg} = 0.398$, $e_0^1 = 0.398$, $e_0^2 = 0.398$, $e_0^3 = 0.398$, $e_0^4 = 0.398$, $e_0^5 = 0.252$, $e_0^6 = 0.159$ and $e_0^7 = 0.124$ (e_0^{vg} and e_0^i denote the initial viscous strains in the glassy branch and the i -th rubbery branch, respectively). It is clear from the figure that dashpots with different relaxation times release their stored viscous strain successively with the increase of the temperature, and all the curves tend to rejoin at their posterior evolution

equilibrium branch. 2. Negative values represent the compressive elastic strain energy.

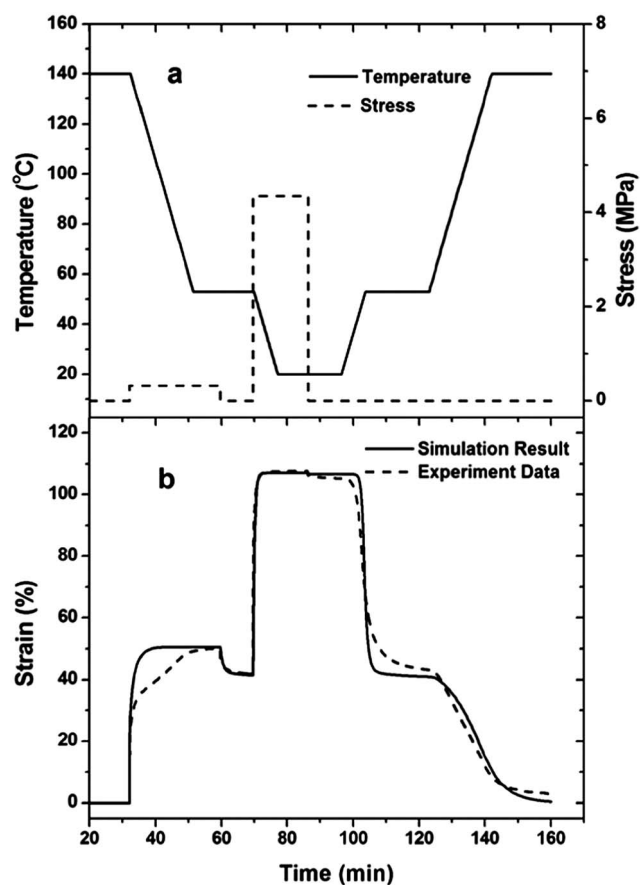


Fig. 5 Triple-SME simulated under stress controlled programming and staged heating recovery conditions. (a) Temperature and stress history. (b) Strain evolution in both simulation and experiment.

Table 1 Parameters of the developed constitutive model

Parameters	Values	Parameters	Values
E_{eq}	0.55 MPa	E_g	1.1 GPa
E_r	0.5 MPa	T_M	35 °C
τ_g	3.71×10^2 s (6.19×10^2 min)	$AF_g k_B^{-1}$	-40 000
τ_i	10^8 s, 10^9 s, 10^{10} s, 10^{11} s, 10^{12} s, 10^{13} s, 10^{14} s or, $1.67 \times (10^6, 10^7, 10^8, 10^9, 10^{10}, 10^{11}, 10^{12})$ min		

process. This is because as the temperature is elevated, the relaxation times in the nonequilibrium branches decrease according to eqn (2) and (3). As the relaxation time in a specific non-equilibrium becomes sufficiently small, observable viscous strain release (recovery) occurs. Since the nonequilibrium branches have different initial relaxation times, they achieve noticeable strain release at different temperatures and times, as shown in Fig. 4a.

At different times of the SM cycle, the elastic strain energy stored in each branch is plotted as histograms in Fig. 4b. For convenience, $t = 0$ is set to be the time when the heating starts, as is the case for the rest of the histograms in the paper. The compressive elastic strain energy is denoted as a negative value for better visualization. As the figure shows, at the end of cooling, the stored elastic strain energies in all branches are positive because of the tensile loading and the stored elastic strain energy

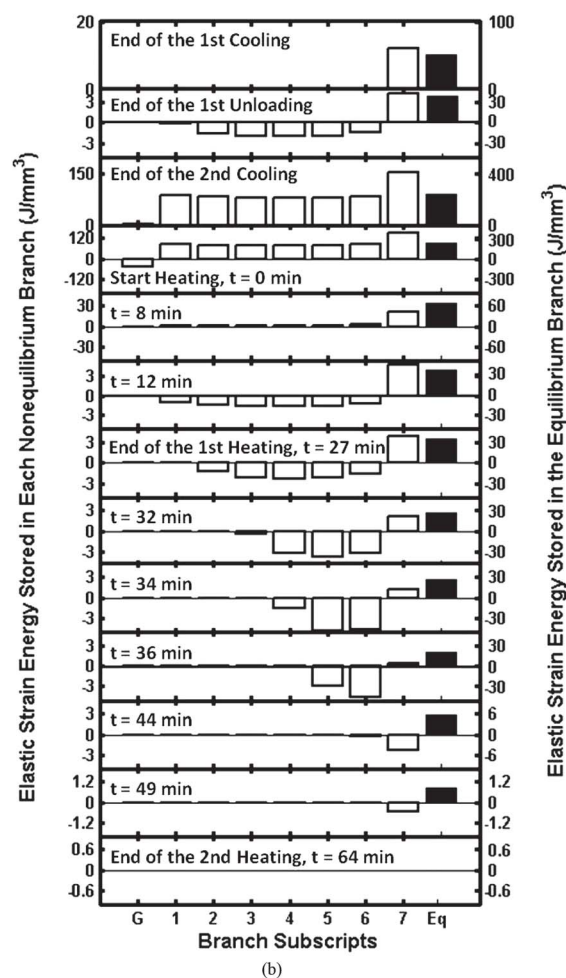
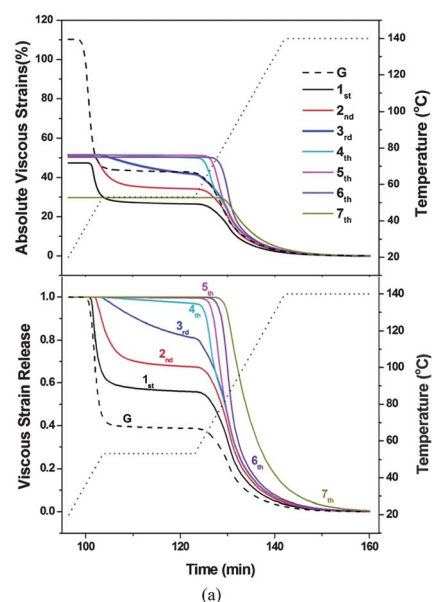


Fig. 6 (a) Strain evolution of dashpots in each rubbery nonequilibrium branch during the free recovery process of triple-SME simulation. The top plot shows the absolute viscous strain and the bottom plot shows the viscous strain release. Key: solid line, strain release degree; dotted line, temperature. (b) Elastic strain energy stored in each rubbery branch during the free recovery process of the triple-SME simulation.

is higher in the branches with longer relaxation times. Removing the external load causes a re-distribution of strains (due to the rebalance of forces to maintain overall equilibrium), and thus elastic strain energy, in all the branches. In particular, the glassy branch is compressed, which resists the tensile stresses in the rest of the branches and fixes the overall strain. At the end of cooling, a slight total energy decrease (a 5.7% drop from 159 J mm^{-3} to 150 J mm^{-3}) is also observed upon unloading. When the heating process begins, the dashpot in each nonequilibrium branch (including the glassy branch) starts to gain mobility. First, the glassy branch releases its compressive strain energy due to its smallest relaxation time. Successively starting from the first rubbery branch, the stretching elastic strain energy first decreases to zero, then becomes compressive in order to maintain the overall stress equilibrium, and finally decays to zero. At the end of heating, only the last rubbery branch has a small amount of compressive strain, which balances the tensile strain in the equilibrium branch. Eventually, the strains in all the branches become zero; the material recovers to its original shape.

3.2 Triple shape memory effect

Triple-SME refers to the phenomenon that a SMP can memorize two temporary shapes in a single shape memory cycle. The triple-shape programming history reported by Xie is replotted in Fig. 5a.³⁰ In the first programming step, the SMP is stretched by a stress of 0.32 MPa at the temperature of $140 \text{ }^\circ\text{C}$. This stress is maintained while the temperature is lowered to $53 \text{ }^\circ\text{C}$ at the rate of $5 \text{ }^\circ\text{C min}^{-1}$. When the temperature reaches $53 \text{ }^\circ\text{C}$, the SMP is equilibrated for 7 min. Afterwards, the external force is removed, which leads to a partial recovery. After 10 min of equilibrium, the remaining (fixed) strain corresponds to the first temporary shape. In the second programming step, the material is stretched by a stress of 4.35 MPa at $53 \text{ }^\circ\text{C}$. The temperature is then lowered to $20 \text{ }^\circ\text{C}$ at $5 \text{ }^\circ\text{C min}^{-1}$ and the external load is maintained for another 7 min before it is removed. This marks the end of the programming process. During recovery, the SMP is heated under a stress-free condition to induce the strain recovery. In the first recovery step, the temperature is ramped to the first recovery temperature of $53 \text{ }^\circ\text{C}$ with a heating rate of $5 \text{ }^\circ\text{C min}^{-1}$ and then held constant for 30 min. Further heating of the SMP to $140 \text{ }^\circ\text{C}$, followed by isothermal holding, leads to a second recovery.

The constitutive model discussed above was applied to the study of triple-SME. It was found that seven rubbery branches, featuring a tenfold sequential increase of relaxation times from $1.67 \times 10^6 \text{ min}$ to $1.67 \times 10^{12} \text{ min}$ in these branches, were sufficient to capture the experimentally observed shape memory behavior. The rest of the material parameters required in the model were simultaneously determined and the final model parameters are listed in Table 1. The simulation results, together with the experimental results (Xie³⁰), are shown in Fig. 5(b).

To reveal the underlying physics of the triple-SM effect, Fig. 6a shows the release of viscous strains in the nonequilibrium branches during the free recovery process. Since the release of the viscous strains in the nonequilibrium branches is closely related to the relaxation times in individual branches, we first look at the relaxation times at the first recovery temperature of $53 \text{ }^\circ\text{C}$, which is also the second deformation temperature. At $53 \text{ }^\circ\text{C}$, relaxation times are $1.91 \times 10^{-3} \text{ min}$ (the glassy branch), 51.5 min (1st

rubbery branch), and $5.15 \times 10^7 \text{ min}$ (7th rubbery branch), respectively. For the glassy branch, its relaxation time is very short. For the 1st rubbery nonequilibrium branch, its 51.5 min relaxation time is in line with the time scale of laboratory physical events (such as free recovery, the second deformation, and other laboratory observations), therefore the dashpots in these two branches play a dominant role at this temperature. For example, deforming the material at this temperature will develop viscous strains in the glassy branch and the 1st rubbery branch. Thus, if the temperature is further lowered, the relaxation time of these two dashpots will increase and the viscous strains developed at $53 \text{ }^\circ\text{C}$ will be memorized. In this regard, the glassy branch and the 1st branch are active for SM behaviors in the second temporary shape. For the 7th branch, however, its relaxation time of $5.15 \times 10^7 \text{ min}$ ($\approx 100 \text{ years}$) is extremely large as compared to the time scale associated with the shape memory events at this temperature. Therefore, the dashpot in the 7th branch can be taken as frozen and the 7th branch can be taken as elastic or inactive for shape memory behaviors. Similar analysis can be carried out for the 2nd to 6th rubbery branches. The importance of relaxation times in individual branches is clearly seen in Fig. 6b, where the release of viscous strains is presented. It can be seen that at $53 \text{ }^\circ\text{C}$, the glassy branch and the first four rubbery branches show a significant release of viscous strains, the rest of the three rubbery branches hold their viscous strains well.

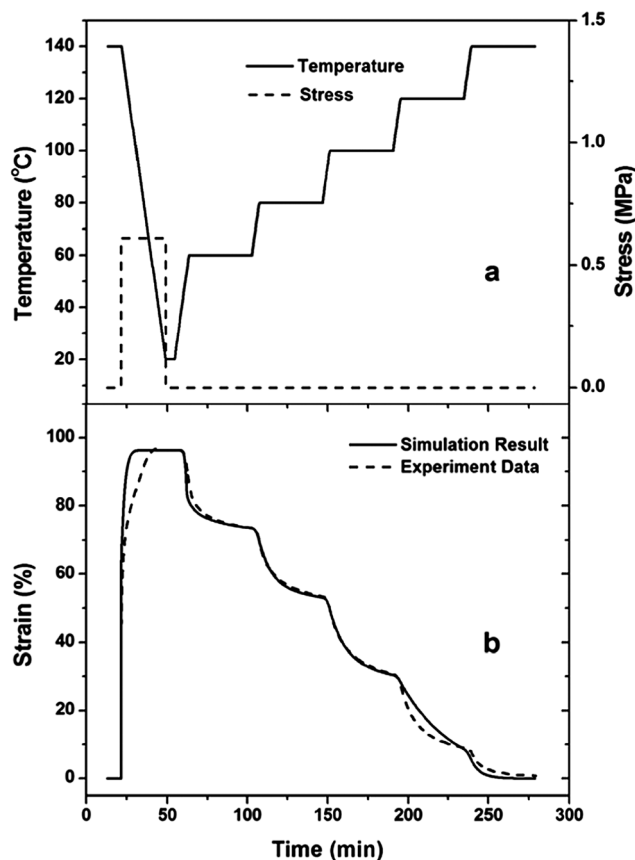


Fig. 7 Multi-SME simulated under stress controlled programming and staged heating recovery conditions. $T_{r1} = 60 \text{ }^\circ\text{C}$, $T_{r2} = 80 \text{ }^\circ\text{C}$, $T_{r3} = 100 \text{ }^\circ\text{C}$, $T_{r4} = 120 \text{ }^\circ\text{C}$, and $T_{r5} = 140 \text{ }^\circ\text{C}$. (a) Temperature and stress history. (b) Strain evolution in both simulation and experiment.

Although results are not shown, it is straightforward to envision that during the mechanical loading in the second programming step, only the dashpots in the glassy branch and the first four rubbery branches deform and the dashpots in the last three rubbery branches are in a dormant state (frozen). Further decreasing the temperature to 20 °C will freeze the viscous deformation in the glassy branches and the first four rubbery branches, which leads to the formation of the second temporary shape. Therefore, the underlying mechanism for the formation of two temporary shapes is that there are different numbers of nonequilibrium branches (or relaxation modes) being active at the two different programming temperatures. At the first programming temperature (140 °C), all the nonequilibrium branches are active; at the second programming temperature (53 °C), only the glassy branch and the first four rubbery branches are active and the last three branches are inactive for the shape memory behavior. It is also noted that, in Fig. 6a, the viscous strains in the glassy branch and the first four rubbery branches are only partially released at 53 °C. The non-released portions of the viscous strains in these dashpots accommodate the unrecovered deformation held by the rest of the rubbery branches, which are SM inactive at this temperature.

The histograms in Fig. 6b show the elastic strain energy stored in the springs of individual branches during the entire shape memory cycle. Under the first deformation temperature of 140 °C, the relaxation times are 3.40×10^{-6} min and 3.40 min for the 1st and 7th rubbery branches, respectively. Because the relaxation times for the six rubbery branches are orders of magnitude shorter than the loading and cooling time (about 20 min in total), significant stress relaxations occur for these non-equilibrium branches. For the 7th branch, whose relaxation time is close to the total time for loading and cooling, only partial stress relaxation occurs. This is evidenced by the histogram at the end of the first cooling where only the 7th branch has some elastic energy stored. After the external stress is removed, springs in the 1–6 nonequilibrium branches tend to be compressed, leading to a redistribution of strains and therefore stored elastic energy in these branches. During the second loading at 53 °C, because the relaxation times in the rubbery branches are long (as discussed above), the stresses in individual branches cannot be relaxed during loading, leading to a significant amount of strain energy in all the individual branches at the end of the second loading.

Similar to the simple SM cycle case, the two unloadings in the triple-SME also cause stored energy loss. In the first unloading at 53 °C, the stored strain energy decreases from 63.4 J mm^{-3} to 48.0 J mm^{-3} , a 24.2% loss. In the second unloading, the energy decreases by 1.2%, from 868.2 J mm^{-3} to 857.2 J mm^{-3} . The large loss at 53 °C is due to the low shape fixity. In particular, because the elastic spring in the glassy branch has the highest modulus, it plays the most important role in shape fixing. When the temperature is high, the dashpot in the glassy branch has a relatively short relaxation time. Therefore, the glassy branch cannot resist the undesirable instantaneous strain recovery. When the temperature is low (at 20 °C), the relaxation time in the glassy branch is extremely long (7.28×10^{436} min or 1.38×10^{431} year). The glassy branch can be taken as an elastic solid with a modulus of the elastic spring in the glassy branch. Therefore, very little instantaneous strain recovery occurs during unloading at 20 °C and the energy loss is small.

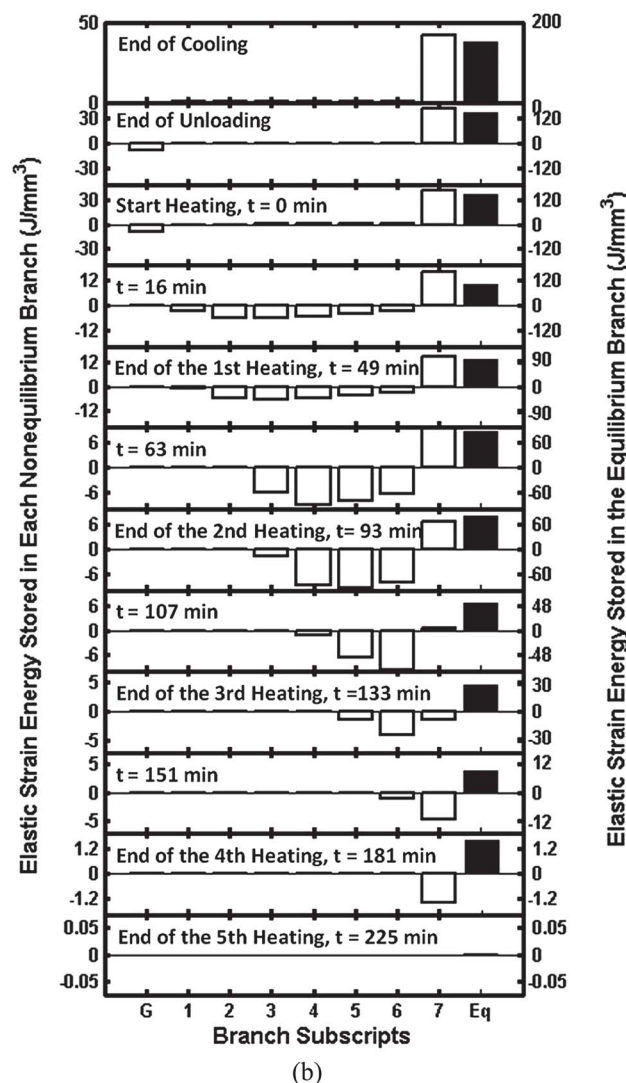
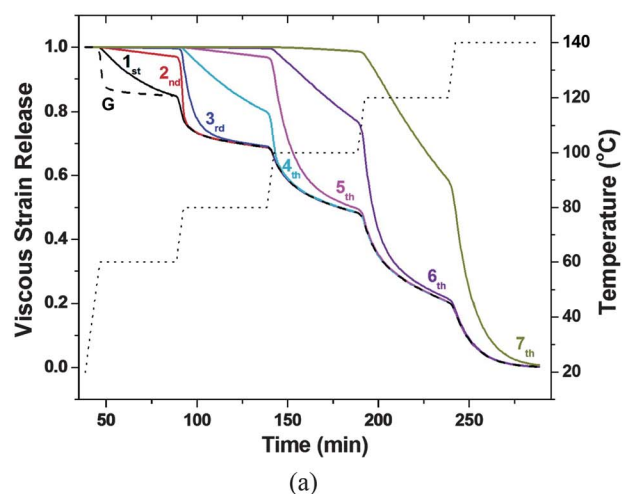


Fig. 8 (a) Strain evolution of dashpots in each rubbery nonequilibrium branch during the free recovery process of multi-SME simulation. Key: solid line, normalized strain release; dotted line, temperature. (b) Elastic strain energy stored in each rubbery branch during the free recovery process of the multi-SME simulation.

Table 2 Relaxation times (in minutes) of individual rubbery branches at different temperatures

Temperature	1	2	3	4	5	6	7
20 °C	3.28×10^{440}	3.28×10^{441}	3.28×10^{442}	3.28×10^{443}	3.28×10^{444}	3.28×10^{445}	3.28×10^{446}
60 °C	6.45×10^{-1}	6.45×10^0	6.45×10^1	6.45×10^2	6.45×10^3	6.45×10^4	6.45×10^5
80 °C	4.35×10^{-3}	4.35×10^{-2}	4.35×10^{-1}	4.35×10^0	4.35×10^1	4.35×10^2	4.35×10^3
100 °C	1.52×10^{-4}	1.52×10^{-3}	1.52×10^{-2}	1.52×10^{-1}	1.52×10^0	1.52×10^1	1.52×10^2
120 °C	1.37×10^{-5}	1.37×10^{-4}	1.37×10^{-3}	1.37×10^{-2}	1.37×10^{-1}	1.37×10^0	1.37×10^1
140 °C	2.24×10^{-6}	2.24×10^{-5}	2.24×10^{-4}	2.24×10^{-3}	2.24×10^{-2}	2.24×10^{-1}	2.24×10^0

In the staged heating process, the release of the elastic strain energy is similar to that in the dual-SM cycle. For individual rubbery branches, the energy is stored in tensile deformations before heating starts. Instead of being released instantaneously, the energy is first transferred and stored in compressive strains, and then gradually released. Therefore, before the stored elastic energy is released, significant energy transfer among different rubbery branches occurs. It is also interesting to note that the first heating not only returns the material to the first temporary shape, it also returns the energy distribution to that after the first unloading event during the programming step. Therefore, the material recovers its energy state in its first temporary shape.

3.3 Multi-shape memory effects

The above mechanism for the triple-shape memory effect can be further extended to the m-SME,³⁰ which refers to the phenomenon that a SMP can memorize multiple (*i.e.* beyond two) temporary shapes in a single shape memory cycle. Fig. 7a shows the thermomechanical history during the shape memory cycle for m-SME. The material is first stretched (stress = 0.65 MPa) at a deformation temperature of 140 °C. This stress is maintained constant during subsequent cooling at a rate of 5 °C min⁻¹. The stress is removed ten minutes after the temperature reaches 20 °C. The SMP is further equilibrated for 10 min. Afterwards, the SMP is heated under a stress-free condition following a multi-stage heating procedure. In each stage, the temperature is ramped to a recovery temperature (T_r) and held constant for 40 min before the next heating process starts. Five recovery temperatures are set as: $T_{r1} = 60$ °C, $T_{r2} = 80$ °C, $T_{r3} = 100$ °C, $T_{r4} = 120$ °C, and $T_{r5} = 140$ °C, and the heating rate is 5 °C min⁻¹.

The model material parameters obtained from fitting triple-SME curves are used to predict the m-SME effect. Fig. 7b shows both model predictions and experimental results. It is clear that the simulation predicts the experimental results very well, indicating that the model is able to capture m-SME.

Fig. 8a shows the relaxation of viscous strains in the rubbery branches during the free recovery process. Similar to the triple-SME, the staged heating leads to a staggered release of viscous strains stored in the dashpots and thus a staggered recovery. This is because the number of active dashpots varies at different recovery temperatures. Table 2 lists the relaxation times of the individual dashpots in the rubbery branches at different temperatures. As discussed above, the so-called SM active or inactive state corresponds to whether or not the branch can develop viscous strain. Therefore, it should be taken in a relative manner depending on the experimental time scale. Here, for the purpose of easy discussion, we use $\sim 10^2$ min relaxation time as the criterion for SM active or inactive state. In Table 2, the SM

inactive branches are marked with italic type. Based on this criterion, at the first staged temperature of 60 °C, only 3 rubbery branches are active. At the second staged temperature of 80 °C, the number of active rubbery branches increases to 5, causing more recovery. At the final temperature of 140 °C, all the rubbery branches become active, leading to a full recovery of the SMP.

Fig. 8b shows the storage and release of elastic energy during the entire shape memory cycle. The trend is similar to those observed in the dual- and triple-shape memory cycles. For the individual rubbery branches, the energy is stored in tensile strains before heating starts. Instead of being released directly, the energy increases first, is stored in compressive strains, and then gradually released. Therefore, before the stored elastic energy is released, significant energy transfer among different rubbery branches occurs. The similarity in the energy transfer and release during the recovery of dual-SME, triple-SME, and m-SME is expected. The difference among these three SMEs is the different heating schemes used during free recovery that can only pause the recovery and therefore energy transfer and release.

4. Conclusions

Recent literature shows that a polymer with a broad thermo-mechanical transition can display a multiple shape memory effect (m-SME), *i.e.* the polymer is capable of memorizing and recovering multiple shapes. This paper reveals quantitatively the physical mechanism and the energy storage and release associated with m-SME by utilizing a multibranch constitutive model, which captures the complex relaxation processes in the polymer. The simulation results, in combination with previously published experimental data, suggest that the m-SME arises from the shifting of individual nonequilibrium branches (or relaxation modes) between a SM active state and a SM inactive state at different programming and recovery temperatures. Due to the complex molecular relaxation, the strain energy stored during shape fixing and released during recovery depends on the deformation temperature, holding time, and cooling time. During free recovery, the stored stress in the individual nonequilibrium branches first reverses its state (for example, from tensile to compression) before it declines to zero.

References

- Z. G. Wei, R. Sandstrom and S. Miyazaki, Shape-memory materials and hybrid composites for smart systems. I. Shape-memory materials, *J. Mater. Sci.*, 1998, **33**(15), 3743–3762.
- C. M. Yakacki, R. Shandas, C. Lanning, B. Rech, A. Eckstein and K. Gall, Unconstrained recovery characterization of shape-memory polymer networks for cardiovascular applications, *Biomaterials*, 2007, **28**(14), 2255–2263.

- 3 A. Lendlein and S. Kelch, Shape-memory polymers as stimuli-sensitive implant materials, *Clin. Hemorheol. Microcirc.*, 2005, **32**(2), 105–116.
- 4 Y. P. Liu, K. Gall, M. L. Dunn, A. R. Greenberg and J. Diani, Thermomechanics of shape memory polymers: uniaxial experiments and constitutive modeling, *Int. J. Plast.*, 2006, **22**(2), 279–313.
- 5 Y. P. Liu, K. Gall, M. L. Dunn and P. M. Cluskey, Thermomechanics of shape memory polymer nanocomposites, *Mech. Mater.*, 2004, **36**(10), 929–940.
- 6 H. Tobushi, H. Hara, E. Yamada and S. Hayashi, Thermomechanical properties in a thin film of shape memory polymer of polyurethane series, *Smart Mater. Struct.*, 1996, **5**(4), 483–491.
- 7 A. Lendlein and S. Kelch, Shape-memory polymers, *Angew. Chem., Int. Ed. Engl.*, 2002, **41**(12), 2035–2057.
- 8 C. Liu, H. Qin and P. T. Mather, Review of progress in shape-memory polymers, *J. Mater. Chem.*, 2007, **17**(16), 1543–1558.
- 9 T. Chung, A. Rorno-Urbe and P. T. Mather, Two-way reversible shape memory in a semicrystalline network, *Macromolecules*, 2008, **41**(1), 184–192.
- 10 K. Gall, C. M. Yakacki, Y. P. Liu, R. Shandas, N. Willett and K. S. Anseth, Thermomechanics of the shape memory effect in polymers for biomedical applications, *J. Biomed. Mater. Res., Part A*, 2005, **73**(3), 339–348.
- 11 P. T. Mather, X. Luo and I. A. Rousseau, Shape memory polymer research, *Annu. Rev. Mater. Res.*, 2009, **39**, 445–471.
- 12 H. Y. Jiang, S. Kelch and A. Lendlein, Polymers move in response to light, *Adv. Mater.*, 2006, **18**(11), 1471–1475.
- 13 H. Koerner, G. Price, N. A. Pearce, M. Alexander and R. A. Vaia, Remotely actuated polymer nanocomposites – stress-recovery of carbon-nanotube-filled thermoplastic elastomers, *Nat. Mater.*, 2004, **3**(2), 115–120.
- 14 A. Lendlein, H. Jiang, O. Jünger and R. Langer, Light-induced shape-memory polymers, *Nature*, 2005, **434**(7035), 879–882.
- 15 M. H. Li, P. Keller, B. Li, X. Wang and M. Brunet, Light-driven side-on nematic elastomer actuators, *Adv. Mater.*, 2003, **15**(7–8), 569–572.
- 16 T. F. Scott, R. B. Draughon and C. N. Bowman, Actuation in crosslinked polymers via photoinduced stress relaxation, *Adv. Mater.*, 2006, **18**(16), 2128–2132.
- 17 T. F. Scott, A. D. Schneider, W. D. Cook and C. N. Bowman, Photoinduced plasticity in cross-linked polymers, *Science*, 2005, **308**(5728), 1615–1617.
- 18 R. Mohr, K. Kratz, T. Weigel, M. Lucka-Gabor, M. Moneke and A. Lendlein, Initiation of shape-memory effect by inductive heating of magnetic nanoparticles in thermoplastic polymers, *Proc. Natl. Acad. Sci. U. S. A.*, 2006, **103**(10), 3540–3545.
- 19 P. R. Buckley, G. H. McKinley, T. S. Wilson, W. Small, W. J. Benett, J. P. Bearinger, M. W. McElfresh and D. J. Maitland, Inductively heated shape memory polymer for the magnetic actuation of medical devices, *IEEE Trans. Biomed. Eng.*, 2006, **53**(10), 2075–2083.
- 20 A. M. Schmidt, Electromagnetic activation of shape memory polymer networks containing magnetic nanoparticles, *Macromol. Rapid Commun.*, 2006, **27**(14), 1168–1172.
- 21 Z. W. He, N. Satarkar, T. Xie, Y. T. Cheng and J. Z. Hilt, Remote controlled multishape polymer nanocomposites with selective radiofrequency actuations, *Adv. Mater.*, 2011, **23**, 3192–3196.
- 22 U. N. Kumar, K. Kratz, W. Wagermaier, M. Behl and A. Lendlein, Non-contact actuation of triple-shape effect in multiphase polymer network nanocomposites in alternating magnetic field, *J. Mater. Chem.*, 2010, **20**, 3404–3415.
- 23 W. M. Huang, B. Yang, L. An, C. Li and Y. S. Chan, Water-driven programmable polyurethane shape memory polymer: demonstration and mechanism, *Appl. Phys. Lett.*, 2005, **86**(11), 114105.
- 24 Y. C. Jung, H. H. So and J. W. Cho, Water-responsive shape memory polyurethane block copolymer modified with polyhedral oligomeric silsesquioxane, *J. Macromol. Sci., Part B: Phys.*, 2006, **45**(4), 453–461.
- 25 T. Pretsch, Triple-shape properties of a thermoresponsive poly(ester urethane), *Smart Mater. Struct.*, 2010, **19**, 015006.
- 26 M. Behl, I. Bellin, S. Kelch, W. Wagermaier and A. Lendlein, One step process for creating triple-shape capability of AB polymer networks, *Adv. Funct. Mater.*, 2009, **19**, 102–108.
- 27 I. Bellin, S. Kelch and A. Lendlein, Dual-shape properties of triple shape polymer networks with crystallizable network segments and grafted side chains, *J. Mater. Chem.*, 2007, **17**, 2885–2891.
- 28 X. F. Luo and P. T. Mather, Triple-shape polymeric composites (TSPCs), *Adv. Funct. Mater.*, 2010, **20**, 2649–2656.
- 29 T. Xie, X. C. Xiao and Y. T. Cheng, Revealing triple-shape memory effect by polymer bilayers, *Macromol. Rapid Commun.*, 2009, **30**, 1823–1827.
- 30 T. Xie, Tunable polymer multi-shape memory effect, *Nature*, 2010, **464**(7286), 267–270.
- 31 J. J. Li and T. Xie, Significant impact of thermo-mechanical conditions on polymer triple-shape memory effect, *Macromolecules*, 2011, **44**, 175–180.
- 32 L. Sun and W. M. Huang, Mechanisms of the multi-shape memory effect and temperature memory effect in shape memory polymers, *Soft Matter*, 2010, **6**, 4403–4406.
- 33 P. Miaudet, A. Derre, M. Mauyse, C. Zakri, P. M. Piccione, R. Inoubli and P. Poulin, Shape and temperature memory of nanocomposites with broadened glass transition, *Science*, 2007, **318**, 1294–1296.
- 34 T. Xie, K. A. Page and S. A. Eastman, Strain-based temperature memory effect for Nafion and its molecular origins, *Adv. Funct. Mater.*, 2011, **21**, 2057–2066.
- 35 K. Kratz, S. A. Madbouly, W. Wagermaier and A. Lendlein, Temperature-memory polymer networks with crystallizable controlling unit, *Adv. Mater.*, 2011, **23**, 4058–4062.
- 36 Y. P. Liu, K. Gall, M. L. Dunn, A. R. Greenberg and J. Diani, Thermomechanics of shape memory polymers: uniaxial experiments and constitutive modeling, *Int. J. Plast.*, 2006, **22**(2), 279–313.
- 37 K. N. Long, M. L. Dunn and H. J. Qi, Mechanics of soft active materials with evolving phases, *Int. J. Plast.*, 2010, **26**, 603–616.
- 38 T. D. Nguyen, H. J. Qi, F. Castro and K. N. Long, A thermoviscoelastic model for amorphous shape memory polymers: incorporating structural and stress relaxation, *J. Mech. Phys. Solids*, 2008, **56**, 2792–2814.
- 39 H. J. Qi, T. D. Nguyen, F. Castro, C. Yakacki and R. Shandas, Finite deformation thermo-mechanical behavior of thermally induced shape memory polymers, *J. Mech. Phys. Solids*, 2008, **56**, 1730–1751.
- 40 G. Barot and I. J. Rao, Constitutive modeling of the mechanics associated with crystallizable shape memory polymers, *Z. Angew. Math. Phys.*, 2006, **57**(4), 652–681.
- 41 H. J. Qi and M. L. Dunn, Thermomechanical Behavior and Modeling Approaches, in *Shape-Memory Polymers and Multifunctional Composites*, ed. J. S. Leng and S. Y. Du, CRC Press/Taylor & Francis Press, 2010.
- 42 L. Sun, W. M. Huang, C. C. Wang, Y. Zhao, Z. Ding and H. Purnawali, Optimization of the shape memory effect in shape memory polymers, *J. Polym. Sci., Part A: Polym. Chem.*, 2011, **46**(16), 3582–3587.
- 43 L. Anand and N. M. Ames, On modeling the micro-indentation response of an amorphous polymer, *Int. J. Plast.*, 2006, **22**(6), 1123–1170.
- 44 T. A. P. Engels, L. C. A. van Breemen, L. E. Govaert and H. E. H. Meijer, Predicting the long-term mechanical performance of polycarbonate from thermal history during injection molding, *Macromol. Mater. Eng.*, 2009, **294**(12), 829–838.
- 45 F. Castro, K. K. Westbrook, K. N. Long, R. Shandas and H. J. Qi, Effects of thermal rates on the thermomechanical behaviors of amorphous shape memory polymers, *Mech. Time-Depend. Mater.*, 2010, **14**, 219–241.
- 46 K. K. Westbrook, P. H. Kao, F. Castro, Y. F. Ding and H. J. Qi, A 3D finite deformation constitutive model for amorphous shape memory polymers: a multi-branch modeling approach for nonequilibrium relaxation processes, *Mech. Mater.*, 2010, **43**, 853–869.
- 47 M. Rubinstein and R. H. Colby, *Polymer Physics*, Oxford University Press, Oxford, New York, 2003.
- 48 P. A. O'Connell and G. B. McKenna, Arrhenius-type temperature dependence of the segmental relaxation below T_g , *J. Chem. Phys.*, 1999, **110**(22), 11054–11060.
- 49 M. L. Williams, R. F. Landel and J. D. Ferry, Temperature dependence of relaxation mechanisms in amorphous polymers and other glass-forming liquids, *Phys. Rev.*, 1955, **98**(5), 1549.
- 50 E. A. Di Marzio and A. J. M. Yang, Configurational entropy approach to the kinetics of glasses, *J. Res. Natl. Inst. Stand. Technol.*, 1997, **102**(2), 135–157.